Analysis of the geopotential from NWM at GNSS sites and its influence in IWV computation

Fernández Laura I.[1,2], Meza Amalia M.[1,2], Natali M. Paula[1,2], and Bianchi Clara E.[1,2]

[1]MAGGIA Lab. Fac. de Cs. Astronómicas y Geofísicas. Univ. Nac. de La Plata. Buenos Aires. Argentina.
[2]CONICET, Argentina.

Correspondence: Laura I. Fernández (lauraf@fcaglp.unlp.edu.ar)

Abstract. Commonly Numerical Weather Models (NWM) users can get the vertically Integrated Water Vapor (IWV) value at a given location from the values at nearby grid points. In this study we used a validated and free available Global Navigation Satellite Systems (GNSS) IWV data set to analyze the very well-known effect of height differences. To this aim, we studied the behavior of 67 GNSS stations in Central and South America with the condition of having a minimum of 5 years of data during the period from 2007 till 2013. The values of IWV from GNSS were compared with the respective values from ERA Interim and MERRA-2 in the same period. Firstly, the total set of stations was compared in order to detect in which cases the geopotential difference between GNSS and NWM deserves a correction. Then, an additive integral correction to the IWV values from ERA Interim was proposed. For the calculation of this correction the multilevel values of specific humidity and temperature given at 37 pressure levels by ERA Interim were used. The performance of the numerical integration method was tested by accurately reproducing the IWV values at each of the grid points surrounding each of the GNSS sites under study. Finally, and considering the IWV_{GNSS} values as a reference, the improvement introduced to the $IWV_{ERAInterim}$ values after adding the corrections is analyzed. In general, the corrections are always recommended but they are not advisable at sea coastal areas or in islands since at least two grid points of the model are usually in the water. In such cases the additive correction could over valuate the IWV.

Keywords: 3394 Instruments and techniques; 6904 Atmospheric propagation; 6964 Radio wave propagation.

1 Introduction

Water vapor is an abundant natural greenhouse gas of the atmosphere. The knowledge of its variability in time and space is very important to understand the global climate system (Dessler et al., 2008). Most of the regional comparisons of IWV from GNSS are aimed at validating the technique by comparing with radiosonde and radiometers where available. A complete example of this is the work of Van Malderen et al. (2014) who compared IWV GPS (Global Positioning System) with IWV derived from ground-based sun photometers, radiosondes and satellite-based values from GOME, SCIAMACHY, GOME-2 and AIRS instruments at 28 sites in the northern hemisphere. Because their comparison is oriented to climatology application, they deal with long-term time series (+ 10 years). The authors asseverate that the mean biases of the GPS with the different instruments vary only between -0.3 and 0.5 $kg\,m^{-2}$ but there are large standard deviations especially for the satellite instruments.

However, some other comparisons examine the IWV_{GNSS} values with respect to the respective estimates from Numerical Weather Models (NWM). If focusing on the application of the current state-of-the-art reanalysis ERA-Interim from the European Centre for Medium-Range Weather Forecasts (ECMWF), both in local and global scale, some recent papers deserve to be mentioned: Heise et al. (2009) used ground pressure data from ECMWF to calculate IWV from 5-minutes Zenith Total Delay (ZTD) at stations without meteorological data available. The authors validate their results with stations with local measurements of pressure and temperature. They also compare IWV from GPS with respect to IWV from ERA-Interim on a global scale. The authors found that IWV from GPS and ECMWF show well agreement on most stations on the global scale except in mountain regions. Moreover they addressed that temporal station pressure interpolation may result in up to 0.5 $kg\,m^{-2}$ IWV uncertainty if a local weather event happened. According to the authors, this phenomenon is observed especially in the tropics and is due to the fact that the ECMWF analysis does not adequately represent the local situation if facing with an increase in the diurnal cycle of surface atmospheric pressure.

Buehler et al. (2012) compare IWV values over Kiruna in the north of Sweden from five different techniques (Radiosondes, GPS, ground-based Fourier-Transform InfraRed (FTIR) spectrometer, ground-based microwave radiometer, and satellite-based microwave radiometer) with IWV from ERA-Interim reanalysis. The processed GPS dataset covers a ten-year period from November 1996 to November 2006. The authors found a good overall agreement between IWV from GPS and from ERA-Interim being the mean of differences 0.29 $\pm$ 1.25 $kg\,m^{-2}$. They also point out that ERA-Interim is drier than the GPS at small IWV values and slightly moister at high IWV values (above 15 $kg\,m^{-2}$).

Ning et al. (2013) evaluate IWV from GPS in comparison with IWV from ERA-Interim and IWV from the regional Rossby Centre Atmospheric (RCA) climate model at 99 European sites for a 14-year period. Because RCA is not an assimilation model, the standard deviation of the difference RCA-GPS resulted 3 times larger than the subtraction ERA-Interim minus GPS. The IWV difference for individual sites varies from -0.21 up to 1.12 $kg\,m^{-2}$ and the corresponding standard deviation is 0.35 $kg\,m^{-2}$. In this work the authors also highlight that the models overestimate IWV for sites near the sea.

Bordi et al. (2014) studied global trend patterns of a yearly mean of IWV from the 20^{th} century atmosphere model (ERA-20CM) and ERA-Interim, both from ECMWF. The authors highlight a regional dipole pattern of inter-annual climate variability over South America from ERA-Interim data. According to this study, the Andean Amazon basin and Northeast Brazil are characterized by rising and decreasing water content associated with water vapor convergence (divergence) and upward (downward) mass fluxes, respectively. Besides, the authors also compared IWV from ERA-Interim with the values estimated at 2 GPS stations in Bogotá and Brasilia. Such comparison on monthly timescale made known a systematic bias attributed to a lack of coincidence in the elevation of the GPS stations and the model grid points.

Tsidu et al. (2015) presented a comparison between IWV from a Fourier Transform InfraRed spectrometer (FTIR, at Addis Ababa), GPS, radiosondes, and ERA-Interim over Ethiopia for the period 2007-2011. The study is focused on the characterization of the different error sources affecting the data time series. In particular, from the study of diurnal and seasonal variabilities, the authors addressed differences in the magnitude and sign of IWV bias between ERA-Interim and GPS. They linked this effect with the sensitivity of the convection model with respect to the topography.

Wang et al. (2015) performed a 12-year comparison of IWV from 3 third generation atmospheric reanalysis models including ERA-Interim, MERRA and the Climate Forecast System Reanalysis (CFSR) on a global scale. IWV values from the reanalysis models were also compared with radiosonde observations in land and Remote Sensing Systems (RSS) on satellites over oceans. The authors asseverate that the main discrepancies of the 3 datasets among them are in Central Africa, Northern South America, and highlands.

In this paper, we investigate the differences between IWV from GNSS by using data products from (Bianchi et al., 2016a) and IWV values given by ERA-Interim and MERRA-2. The comparison was performed taking into account the geopotential differences (Δz) between each GNSS station and the correspondent values assigned by the models. We proposed an additive numerical correction to the IWV from NWM and the strategy was tested for ERA-Interim re-analysis model. Section 2 describes the different sets of data used in this study. Follows the explanation of the methodology and the presentation of the results obtained after applying the proposed correction to IWV values from ERA-Interim.

2 Data

2.1 IWV from GNSS

The GNSS data is the main source of information for the spatial and temporal distribution of water vapor. Thus, the main variable considered is the IWV estimated from the delay caused by the troposphere to the GNSS radio signals during its travel from the satellite to the ground receiver. The total delay projected onto the zenith direction (ZTD) is usually split into two contributions: the hydrostatic delay (ZHD, Zenith Hydrostatic Delay) depending merely on the atmospheric pressure and the Zenith Wet Delay (ZWD) depending mainly on the humidity. The IWV_{GNSS} can be obtained from ZWD multiplying it by a function of the mean temperature of the atmosphere.

The reference database of IWV_{GNSS} used in this study comes from a geodetic processing over 136 tracking stations in the American Continent placed from southern California to Antarctica (see Figure 1), during the 7-year period from January 2007 till December 2013 (Bianchi et al., 2016b). Specifically, the data series of IWV_{GNSS} used here is restricted to those 67 stations with IWV time series spanning more than 5 years (see Figure 1 and Table 1). More details of the steps, models and conventions followed by the geodetic processing to obtain the IWV_{GNSS} values are in Bianchi et al. (2016a).

2.2 IWV from NWM

The values of columnar Integrated content of Water Vapor (IWV) as reanalysis products from ERA-Interim (Dee et al., 2011) and MERRA-2 (GMAO, 2015;Bosilovich et al., 2015;Gelaro et al., 2017) were evaluated in this study. The horizontal resolutions are $0.25° \times 0.25°$ for ERA-Interim and $0.625° \times 0.50°$ for MERRA-2, respectively. Because ERA-Interim data is given 4 times a day, in order to perform the comparison and even if MERRA-2 gives hourly data, we pick up IWV data from MERRA-2 every 6 hours at 0, 6, 12 and 18 hours of Universal Time (UT). Thus, to be able to carry out the comparison, MERRA-2 was only partially evaluated.

ERA-Interim is the global atmospheric reanalysis produced by the European Centre for Medium-Range Weather Forecasts (ECMWF). It covers the period from 1979 up to today and supersedes the ERA-40 reanalysis. ERA-Interim address some difficulties of ERA-40 in data assimilation mainly related to the representation of the hydrological cycle, the quality of the stratospheric circulation, and the consistency in terms of reanalyzed geophysical fields (Dee et al., 2011).

MERRA-2 is the successor of The Modern-Era Retrospective Analysis for Research and Applications (MERRA) from NASA's Global Modeling and Assimilation Office (Rienecker et al., 2011). MERRA-2 represents a quality improvement compared with MERRA because of the trends and jumps linked to changes in the observing systems. Additionally, MERRA-2 assimilates observations not available to MERRA and reduces bias and imbalances in the water cycle (Gelaro et al., 2017). Moreover, the longitudinal resolution of MERRA-2 data is changed from 0.667° in MERRA to 0.625° whereas the latitudinal resolution remains unchanged (0.5°) (Bosilovich et al., 2015).

To this application we used two different data sets. First, the gridded values of the vertical Integral of Water Vapor (IWV) from both re-analysis models. Because the comparison is performed at each GNSS station, a bi-linear interpolation of each gridded data set was performed. Moreover, IWV data is given at the correspondent geopotential invariant for each model. In addition, we also use vertical values of air temperature (T) and specific humidity (q) from ERA-Interim for the calculation of the correction to the IWV values. These variable, q and T, are also gridded and given in 37 levels of atmospheric pressure from 1 to 1000 hPa. This second set of data will be used for the calculation of the integral correction that will be developed in the following section.

3 Methodology

As mentioned before, even when both reanalysis models give grid values of the vertical integral of the water vapor, the solution provided by each model is linked to its respective geopotential surface invariant. Nevertheless, elevation differences between geopotential from each model grid and computed from GNSS height must be addressed.

We have to remember that the difference between geopotential (in $m^2\ s^{-2}$) and geopotential height (in m) is $g_0 = 9.80665\ m\,s^{-2}$ the normal gravity acceleration at 45° latitudes. Thus, assuming that the integral of the water vapor is computed from topside and downwards, if the height of a given point from a model is located lower than the position of the receiver, the model integrates a larger column of water vapor and the opposite if the model locates upper than it.

We performed the present comparison establishing a selection criterion according to the difference of geopotential (z) between each reanalysis model and GNSS at the station.

In order to compute the geopotential of the GNSS stations (z_{GNSS}) we followed van Dam et al. (2010) algorithm. Because the geodetic coordinates ($\phi,\ \lambda,\ h$) of the GNSS site are known, we obtained the orthometric height (H) at each GNSS station by correcting the ellipsoidal height with the EGM08 model (Pavlis et al., 2012). Thus, the geopotential is (van Dam et al., 2010)

$$z_{GNSS} = \frac{g_s(\phi)\, C(\phi)\, H}{(C(\phi) + H)} \tag{1}$$

where the radius of the ellipsoid at geodetic latitude ϕ is,

$$C(\phi) = \left(\frac{cos^2(\phi)}{a^2} + \frac{sin^2(\phi)}{b^2} \right)^{-1/2} \tag{2}$$

with $a = 6378137m.$ and $b = 6356752.3142m.$ are the semimajor and semiminor axis of the WGS84 ellipsoid, respectively (Hofmann-Wellenhof and Moritz, 2006). Moreover, the value of the gravity on the ellipsoid at geodetic latitude ϕ can be written as (van Dam et al., 2010).

$$g_s(\phi) = g_E \frac{1 + k_s\ sin^2(\phi)}{\sqrt{1 - e^2\ sin^2(\phi)}} \tag{3}$$

with $e^2 = 0.00669437999014$ is the first eccentricity squared of the WGS84 ellipsoid and $g_E = 9.7803253359m\ s^{-2}$ is the normal gravity at the Equator (Hofmann-Wellenhof and Moritz, 2006) and $k_s = 0.001931853$ (van Dam et al., 2010).

For a given GNSS station, the respective geopotential from each of the 2 reanalysis models resulted from a bi-linear interpolation of the respective invariant static geopotential at the 4 grid points around the GNSS site. Because the points of the NWM grid surrounding the GNSS station have different geopotential values and those values are in turn different from z_{GNSS}, we propose to correct on each of these 4 points. Thus, if Δz^i refers to the difference between z_{GNSS} and z_{NWM} in each of those of the 4 grid points,

$$\Delta z^i = z_{GNSS} - z^i_{NWM}, i = 1, 2, 3, 4. \tag{4}$$

where NWM corresponds to ERA-Interim or MERRA-2.

We will then propose a correction procedure that, compensating Δz^i in each of the 4 grid points, corrects its values of IWV_{NWM}. After "moving" the grid points to z_{GNSS}, a bi-linear interpolation is performed to obtained the corrected value of IWV at the location of the GNSS site. In brief, this procedure is equivalent to lifting (or descending as appropriate) each of the grid points in order to build up a plane at z_{GNSS}.

Prior to the correction, we analyze the performance of ERA-Interim and MERRA-2 with respect to GNSS. Thus, although IWV_{GNSS} is produced every half hour and $IWV_{MERRA-2}$ is available hourly, we consider only the epochs when ERA Interim data is available to perform the comparison at 0, 6, 12 and 18 UT. Table 2 shows the mean values of IWV from GNSS ($\overline{IWV}_{GNSS}$) during the period 2007-2013 and its standard deviation for all the stations. We assume that the static geopotential from the NWM at each GNSS site (z_{NWM}) is obtained from a bi-linear interpolation of the static geopotential at the 4 grid points surrounding it (z^i_{NWM}). Thus, Table 2 shows the geopotential difference ($\Delta z = z_{GNSS} - z_{NWM}$) in addition to the respective differences of the mean values ($\Delta\overline{IWV} = \overline{IWV}_{GNSS} - \overline{IWV}_{NWM}$), where NWM indicates ERA Interim and MERRA-2. All the averages are computed over the period 2007-2013.

In general when regarding at Table 2, we can observe that the best agreements between the average IWV values from GNSS and the average from the models are where the Δz are small (for example: CONZ, VITH, SMAR, LPGS, MAPA, SCUB among others). In other words, in general the NWMs represent very well the IWV values ($\Delta\overline{IWV}$ < 1.5 $kg\ m^{-2}$) if $|\Delta z|$ is small. That means, the geopotential difference is in the order of 500 $m^2\ s^{-2}$ at most.

On the other hand, The difference of the model representation of the IWV with respect to GNSS grows as the height differences (Δz) become larger and this is true for all values of $\overline{IWV}_{GNSS}$. As an example we can mention the cases of SANT ($\overline{IWV}_{GNSS} \sim 12\ kg\ m^{-2}$, $|\Delta z| > 10000\ m^2\ s^{-2}$) and CUCU ($\overline{IWV}_{GNSS} \sim 43\ kg\ m^{-2}$, $|\Delta z| \sim 8000\ m^2\ s^{-2}$).

However, other than these cases that can be considered critical, the differences are also important in those sites with moderate $|\Delta z|$ (larger that 500 $m^2\ s^{-2}$) and $\overline{IWV}_{GNSS} > 20 kg^{-2}$ (CEFE, BRAZ, RIOD, GUAT).

Note that some MERRA-2 differences values could be a little bigger than ERA Interim ones and this would be expected because of the coarser grid. However, this is not a general rule and some stations are in fact better represented by MERRA-2 with $|\Delta z|$ and $\left|\Delta\overline{IWV}\right|$ smaller than ERA Interim even if they are located in highlands (see SANT, COPO).

Figure 2 (up) shows the geopotential differences (Δz) as a function of the mean IWV values from GNSS ($\overline{IWV}_{GNSS}$). Results for MERRA-2 are on the left and the same for ERA Interim on the right. Different colors mean negative $\Delta\overline{IWV}$ in blue and positive $\Delta\overline{IWV}$ in red. While the red dots indicate differences greater than 2.5 $kg\ m^2$, the intermediate differences between 0 and 2.5 $kg\ m^2$ are in a red degrade. Similarly, the blue dots show differences less than -2.5 $kg\ m^2$ and the differences between -2.5 and 0 $kg\ m^2$ are in a blue degrade.

It is assumed that these different values of $\Delta\overline{IWV}$ are due to the geopotential difference. Therefore, they commonly carry the opposite sign to the Δz as we expect. However there are some cases where $\Delta\overline{IWV}$ have the same sign as Δz evidencing that the reanalysis models can overvalue or undervalue the value of $\overline{IWV}$ in the station and this should not be due to Δz.

Because $\Delta\overline{IWV}$ is nothing but the difference between mean values from GNSS and NWM, a negative value for negative Δz indicate an overestimation by the reanalysis model and on the contrary, the underestimation by the model is shown with red dots where Δz is positive.

Therefore, figure 2 (up) can reveal the average behaviour of the reanalysis models with respect to GNSS for the period 2007-2013 in the region. Comparing both figures 2 and focusing on $\Delta z \pm$ 2000 $m^2\ s^{-2}$, we can see on the right (MERRA-2) many blue points in the interval from -2000 to 0 $m^2\ s^{-2}$ (a little less than 20% of the total number of stations). On the contrary, in figure 2 left (ERA Interim) only 12% of the stations show this behaviour. All these points have $\overline{IWV}_{GNSS}$ < 20 $kg\ m^2$ and the differences $\Delta\overline{IWV}$ for ERA Interim are between -1 and 0 $kg\ m^2$ smaller than the same differences for MERRA 2. Thus, we can see an overestimation for MERRA-2.

On the other hand if we analyze the red dots that are located for Δz between 0 and 2000 $m^2\ s^{-2}$, we can see the trend is the opposite. MERRA 2 underestimates 6% of stations while ERA Interim underestimates 12% of sites. However, the differences $\Delta\overline{IWV}$ never exceed 1 $kg\ m^2$.

Figure 2 (down) shows the spatial distribution of $\Delta\overline{IWV}$ for MERRA-2 (left) and ERA Interim (right). If we take as reference the RNNA station in both maps (see station number 51 in Figure 1), and advancing towards the south along the Atlantic coast, the behavior of both models results similar. Both reanalysis are dryer than GNSS and this same effect is seen in the southern mountainous areas. However, going along the Atlantic coast from RNNA to the north and up to the Amazon river we can see different behaviours of the reanalyses, while ERA Interim continues to underestimate IWV_{GNSS}, MERRA-2 shows to be wetter than GNSS. The overall agreement between GNSS and MERRA-2 is -0.39 $\pm$ 2.77 and between GNSS and ERA Interim is 0.13 $\pm$ 2.52. Being these values the result of an average over all the $\Delta\overline{IWV}$ differences.

These findings show that MERRA-2 resulted wetter than GNSS while ERA Interim is slightly dryer than GNSS in Central and South America. This is in agreement with the findings of Buehler et al. (2012), who found out that the mean value of the differences between IWV from GPS and ERA is 0.28 $\pm$ 1.25 for a high latitude location in Sweden, revealing also an underestimation of the reanalysis model.

Finally, the correlation coefficients between $\overline{IWV}_{GNSS}$ values and the respective ones for both NWM, are higher than 0.95 in most of the cases (not shown).

3.1 Computation of the integral correction

Following we proceed to compensate the IWV_{NWM} at each of the grid points. The correction will be calculated only for one of the two re-analysis models tested. We have chosen ERA Interim over MERRA 2 for the calculation and testing of these corrections not only because ERA Interim has a thinner grid, but also considering the results of Zhu (2014). Effectively, Zhu (2014) compare several reanalysis projects with independent sounding observations recorded in the Eastern Himalayas during June 2010. Among all the reanalysis models ERA-Interim and MERRA, the predecessor of MERRA 2 were included. The authors analyze temperature, specific humidity, u-wind, and v-wind between 100 hPa and 650 hPa. The authors found that ERA-Interim showed the best performance for all variables including specific humidity the key variable to produce the integrated water vapor.

Thus, we used air temperature (T) and specific humidity (q) on 37 atmospheric pressure levels from ERA-Interim data to compute the proposed correction.

As we mentioned before, the GNSS geopotential (z_{GNSS}) is set as a reference, and the value of the geopotential from ERA-Interim ($z^i_{ERAInterim}$) at each of the 4 grid points surrounding the GNSS site are not the same but may differ several hundred meters. Commonly, neither z_{GNSS} nor the geopotential at any of the 4 grid points matches the geopotential of the nearby pressure level. Therefore, the values of all parameters in the adjacent levels must be used to interpolate (or extrapolate) pressure, temperature and specific humidity in the unknown geopotential ($z_{GNSS} and z^i_{ERAInterim}$).

Thus, the expression of the pressure at an unknown geopotential (z_i) with respect to a given reference data level (z_0) is (van Dam et al., 2010)

$$p(z_i) = p_0 \left(\frac{T_0 - \lambda\, \delta z}{T_0} \right)^{g_0/R\lambda} \tag{5}$$

where T_0 and p_0 refer to the temperature and pressure values at a reference level z_0, $R = 287.04\ J\ kg^{-1}\,^\circ K$ is the gas constant and $\lambda = 0.006499\,^\circ K\ m^{-1}$ is the lapse rate of the temperature, and δz is the geopotential difference between z_i and the reference level z_0. Notice that δz is different of Δz, where the Δz refers to the difference between z_{GNSS} and z_{NWM}. The numerator of Eq. (5) is the temperature estimated at the desired geopotential z_i assuming that the temperature decreases with altitude according to λ. This expression is used to compute p at both z_{GNSS} and each of the grid points of the model ($z^i_{ERAInterim}$). Finally, the specific humidity (q) is also estimated at the desired z_i by a linear interpolation (extrapolation) from data at the adjacent layers.

After knowing p, T and q at each geopotential, z_{GNSS} and the 4 grid points of $z^i_{ERAInterim}$, we can estimate the necessary corrections to the grid points. Such additive corrections to the IWV values at the grid points are equivalent to move the static geopotential of the grid to the z_{GNSS}. Then, the corrected IWV_{NWM} is obtained at the GNSS site by a bi-linear interpolation of the 4 corrected values.

Because each value of IWV provided by ERA-Interim is the result of the numerical integration of the expression (Berrisford et al., 2011).

$$IWV_{ERAInterim} = \frac{1}{g_0} \int_{p_1}^{p_s} q(p)\, dp \tag{6}$$

where g_0 is the standard acceleration of the gravity at mean sea level, $q(p)$ is the specific humidity of the air at the pressure level p and the integral is calculated from the first level (p_1) up to the model surface level (p_s), i.e. up to the static geopotential that corresponds to the station.

Thus, the proposed correction can generally be written by:

$$\Delta IWV = \frac{1}{g_0} \sum_{i=A}^{B} \frac{q_{i+1} + q_i}{2} (p_{i+1} - p_i)\, (-1)^n \begin{cases} n = 1 & if \quad p_{GNSS} < p_{NWM} \\ n = 2 & if \quad p_{GNSS} > p_{NWM} \end{cases} \tag{7}$$

where the NWM is ERA Interim, A corresponds to the highest z (z_{GNSS} or z^i_{NWM}) and B the lowest z; q_i and p_i are q and p at z_i and q_{i+1} and p_{i+1} are q and p at z_{i+1}, respectively. The values of p grows downwards resulting p_1 = 1 hPa. and p_{37}= 1000 hPa. This quantity have to be additive if $z_{GNSS} < z^i_{NWM}$ or subtractive if opposite and the sign is determined by n.

If z_{GNSS} and z^i_{NWM} are at the same level, equation (7) is reduced to

$$\Delta IWV = \frac{1}{g_0} \frac{q_{GNSS} + q_{NWM}}{2} (p_{GNSS} - p_{NWM}) \tag{8}$$

where q_{GNSS} is q at z_{GNSS} and q_{NWM} is q at the static geopotential of the grid point (z^i_{NWM}). The sign is determined by $\Delta p = p_{GNSS} - p_{NWM}$ and the sum of the intermediate terms results null in this case.

Figure 3 illustrates the application of the correction to an example. In a given instant, we know the geopotential of the GNSS station and the static geopotential assigned by the NWM to the 4 grid points surrounding it (z_{GNSS} and z^i_{NWM}, i=1,2,3,4). We also know the geopotential at 37 pressure levels (z_{level}) from 1 hPa till 1000 hPa, as well as specific humidity (q) and temperature (t) at these levels. We should consider that at any time the pressure value of each level is constant but it does not necessarily happen the same with the geopotential height.

We take just 1 of the 4 grid points and lets suppose that both unknowns (z^i_{NWM} and z_{GNSS}) are located between the levels 27 (750 hPa) and 28 (775 hPa). Thus, we could use the available data at levels 27 and 28 along with Eq. (5) and the before mentioned considerations to estimate p, t and q at z^i_{NWM} and z_{GNSS}. Finally, ΔIWV is computed by means of Eq. (8) for this example.

4 Results

Before analyzing the results of the correction process explained in the previous section, we will present a validation of the numerical integration method used. To this end, we calculate the values $IWV_{ERAInterim}$ at each grid point by using the numerical integral of the equation 6. The integration limits range from 1 hPa to the static geopotential value assigned by the model to the point ($z^i_{ERAInterim}$). Table 3 shows the good results obtained with this procedure. In each grid point the mean value of the differences ($IWV_{ERAInterim}$ data - $IWV_{ERAInterim}$ calculated) is presented. Standard deviations are also shown. It can be seen that in general the values are resulted very close to zero.

In order to evaluate the improvements introduced by the correction, we can see in Figure 4 (left) Δz plotted as a function of IWV mean values from GNSS ($\overline{IWV}_{GNSS}$). Now the different color dots show the magnitude of $\left|\Delta\overline{IWV}\right|$

$$\left|\Delta\overline{IWV}\right| = \left|\overline{IWV}_{GNSS} - \overline{IWV}_{ERAInterim}\right| \tag{9}$$

where the color code is: green for differences under 1 $kg\ m^{-2}$, light blue for 1 $kg\ m^{-2} \leq \left|\Delta\overline{IWV}\right| \leq 1.5\ kg\ m^{-2}$, orange dots represent $1.5\ kg\ m^{-2} < \left|\Delta\overline{IWV}\right| \leq 2.5\ kgm^{-2}$ and finally red dots are $\left|\Delta\overline{IWV}\right| \geq 2.5\ kg\ m^{-2}$. Figure 4 (right) shows the situation after applying the proposed integral correction to ERA Interim data. Here we can clearly see a general improvement and the elimination of the red dots, which indicated the maximum discrepancies.

Notice that where $\left|\Delta\overline{IWV}\right| \leq 1.5\ kg\ m^{-2}$ before the correction, even though the differences improve, they are still small. However, a significant improvement is evident in those stations with $\left|\overline{IWV}\right| < 20\ kg\ m^{-2}$ and $|\Delta z| > 2000\ m^2\ s^{-2}$. In addition, the situation also improves for stations with $\left|\overline{IWV}\right| > 20\ kg\ m^{-2}$ and $|\Delta z| > 500\ m^2\ s^{-2}$.

The good performance of the proposed correction can also be seen in Figure 5. The plots are arranged in two columns where the left column shows stations with positive Δz, it means that GNSS station is higher to the location assigned by ERA-Interim. Accordingly, the model integrates a thicker layer of atmosphere and thus $IWV_{ERAInterim}$ values resulted larger than ones from IWV_{GNSS}. The opposite (Δz is negative) is represented by the sites at the right column. Moreover, the differences in Δz are presented decreasing from top to bottom in each column.

We can see that the most important corrections are at BOGT in Bogotá, Colombia, and SANT in Santiago de Chile, Chile. In this examples the differences ($IWV_{GNSS} - IWV_{ERAInterim}$), which can reach up to 7 $kg\ m^{-2}$, are significantly reduced.

However the application of this correction, in some cases, should be precautionary. Effectively, sometimes different shortcomings of the model overlap the height problem and therefore the proposed correction could not work. As an example of this we can mention the case of coastal and/or insular stations where 2 or more grid points will be in the ocean. In all these cases the value of IWV calculated from the bi-linear interpolation will be overvalued. Let's analyze in detail the case of stations near the seashore (for example PARC in Punta Arenas, Chile) where 2 of the 4 grid points are in the ocean (see Figure 6). Also Δz = -1271.86 in PARC indicating that the geopotential from ERA Interim is larger than the GNSS geopotential and therefore the proposed correction will be additive. Besides this result, the $IWV_{ERA-Interim}$ resulted over-estimated by applying a bi-linear interpolation that uses data points in the ocean. In conclusion, the value ($IWV_{ERA-Interim} + correction$) will result larger than the IWV_{GNSS} value that you intend to estimate. Thus, this is an example where applying the suggested correction may worsen the results. The same situation is presented in RIO2 at the Argentinean Atlantic coast.

5 Discussion and Conclusions

The NWM users commonly utilize the IWV values on a grid and calculate with them the IWV value at the desired place by using some interpolation method.

In this work, taking the values of IWV_{GNSS} as reference, we show that there are cases where the IWV values obtained from the NWM have differences of several $kg\,m^{-2}$ and these discrepancies are mainly due to the difference in geopotentials. We analyzed the discrepancies between the vertically Integrated Water Vapor values provided by two re-analysis models (ERA-Interim and MERRA-2) with respect to the IWV_{GNSS} values taken as a reference in the South and Central American continent for the period 2007-2013. The results of this comparison allow us to ensure that MERRA-2 resulted wetter than GNSS while ERA Interim is slightly dryer. In addition, when geopotential differences are moderate or large ($|\Delta z|$ > 500 $m^2\,s^{-2}$) discrepancies are still important in those stations with $\overline{IWV}$ > 20 $kg\,m^{-2}$.

Several authors had been reported problems related to the elevation correction for data from the reanalysis models. The artificial bias in IWV introduced by this altitude difference was previously reported by Bock et al. (2007);Van Malderen et al. (2014);Bordi et al. (2014) and Bianchi et al. (2016a). Moreover, this effect can also affect other variables. For instance, Gao et al. (2012) studied the height corrections for the ERA-Interim 2m-temperature data at the Central Alps and they also found large biases that must be corrected in mountainous areas. Some other authors, also studied the tropospheric refraction effects on space geodetic techniques by considering this effect. For example, Teke et al. (2013) performed an inter-technique comparison of ZTD in the framework of 4 continuous Very Long Baseline Interferometry (VLBI) campaigns also including NWM and taking into account the effect of the height differences.

We proposed an integral correction that compensates the effect of the geopotential difference between GNSS and the interpolated grid points in the reanalysis model and the results were tested with the respective ones from ERA-Interim. The correction is computed as the numerical integration of the specific humidity where the integral limit is a pressure difference at Δz (see Eqs. 7 and 8). The application of the numerical correction successfully reduced the differences between IWV_{GNSS} and $IWV_{ERAInterim}$ significantly. We can also highlight that for more than 90 $\%$ of the stations studied resulted $\Delta\overline{IWV}$ < 1.5 $kg\,m^{-2}$ after applying it.

Author contributions. L.I. Fernández led the study and contributed to data collection, analysis, and interpretation of the results; A.M. Meza and M.P. Natali co-wrote the paper. They also contributed to the statistical analysis and the interpretation of the results. C. E. Bianchi contributed to data collection. All authors read and approved the final manuscript.

Competing interests. The authors declare that they have no conflict of interest.

Acknowledgements. This research was supported by the National Scientific and Technical Council of Argentina (CONICET) PIP 112-201201-00292 and La Plata National University (UNLP) project 11G/142. We would also like to thank the people, organizations and agencies responsible to collect, compute, maintain and openly provide the observations and the products employed in this work: The European Centre for Medium-Range Weather Forecasts (ECMWF) for providing the ERA-Interim reanalysis data (http://apps.ecmwf.int/datasets/). and the Global Modeling and Assimilation Office (GMAO) from National Aeronautics and Space Administration (NASA, USA) for providing MERRA-2 data (https://gmao.gsfc.nasa.gov/reanalysis/MERRA-2/).

References

Berrisford, P., Kållberg, P., Kobayashi, S., Dee, D., Uppala, S., Simmons, A. J., Poli, P., and Sato, H.: Atmospheric conservation properties in ERA-Interim, Quarterly Journal of the Royal Meteorological Society, 137, 1381–1399, https://doi.org/10.1002/qj.864, 2011.

Bianchi, C. E., Mendoza, L. P. O., Fernández, L. I., Natali, M. P., Meza, A. M., and Moirano, J. F.: Multi-year GNSS monitoring of atmospheric IWV over Central and South America for climate studies, Annales Geophysicae, 34, 623–639, https://doi.org/10.5194/angeo-34-623-2016, 2016a.

Bianchi, C. E., Mendoza, L. P. O., Fernández, L., Natali, M. P., Meza, A., and Moirano, J.: Time series of atmospheric water vapour and troposphere zenith total delay, over Central and South America, from a homogeneous GNSS reprocessing (MAGGIA ZTD & IWV Solution 1), https://doi.org/10.1594/PANGAEA.858234, https://doi.org/10.1594/PANGAEA.858234, supplement to: Bianchi, C et al. (2016): Multi-year GNSS monitoring of atmospheric IWV over Central and South America for climate studies. Annales Geophysicae, 34(7), 623-639, https://doi.org/10.5194/angeo-34-623-2016, 2016b.

Bock, O., Bouin, M.-N., Walpersdorf, A., Lafore, J. P., Janicot, S., Guichard, F., and Agusti-Panareda, A.: Comparison of ground-based GPS precipitable water vapour to independent observations and NWP model reanalyses over Africa, Quarterly Journal of the Royal Meteorological Society, 133, 2011–2027, https://doi.org/10.1002/qj.185, 2007.

Bordi, I., Bonis, R. D., Fraedrich, K., and Sutera, A.: Interannual variability patterns of the world's total column water content: Amazon River basin, Theoretical and Applied Climatology, 122, 441–455, https://doi.org/10.1007/s00704-014-1304-y, 2014.

Bosilovich, M. G., Lucchesi, R., and Suarez, M.: MERRA-2: File Specification, https://ntrs.nasa.gov/search.jsp?R=20150019760, 2015.

Buehler, S. A., Östman, S., Melsheimer, C., Holl, G., Eliasson, S., John, V. O., Blumenstock, T., Hase, F., Elgered, G., Raffalski, U., Nasuno, T., Satoh, M., Milz, M., and Mendrok, J.: A multi-instrument comparison of integrated water vapour measurements at a high latitude site, Atmospheric Chemistry and Physics, 12, 10 925–10 943, https://doi.org/10.5194/acp-12-10925-2012, https://www.atmos-chem-phys.net/12/10925/2012/, 2012.

Dee, D. P., Uppala, S. M., Simmons, A. J., Berrisford, P., Poli, P., Kobayashi, S., Andrae, U., Balmaseda, M. A., Balsamo, G., Bauer, P., Bechtold, P., Beljaars, A. C. M., van de Berg, L., Bidlot, J., Bormann, N., Delsol, C., Dragani, R., Fuentes, M., Geer, A. J., Haimberger, L., Healy, S. B., Hersbach, H., Hólm, E. V., Isaksen, L., Kållberg, P., Köhler, M., Matricardi, M., McNally, A. P., Monge-Sanz, B. M., Morcrette, J.-J., Park, B.-K., Peubey, C., de Rosnay, P., Tavolato, C., and Thépaut, J.-N.; Vitart, F.: The ERA-Interim reanalysis: configuration and performance of the data assimilation system, Quarterly Journal of the Royal Meteorological Society, 137, issue 656, 553–597, https://doi.org/10.1002/qj.828, 2011.

Dessler, A. E., Zhang, Z., and Yang, P.: Water-vapor climate feedback inferred from climate fluctuations, 2003–2008, Geophysical Research Letters, 35, https://doi.org/10.1029/2008gl035333, 2008.

Gao, L., Bernhardt, M., and Schulz, K.: Elevation correction of ERA-Interim temperature data in complex terrain, Hydrology and Earth System Sciences, 16, 4661–4673, https://doi.org/10.5194/hess-16-4661-2012, https://www.hydrol-earth-syst-sci.net/16/4661/2012/, 2012.

Gelaro, R., McCarty, W., Suárez, M. J., Todling, R., Molod, A., Takacs, L., Randles, C. A., Darmenov, A., Bosilovich, M. G., Reichle, R., et al.: The modern-era retrospective analysis for research and applications, version 2 (MERRA-2), Journal of Climate, 30, 5419–5454, 2017.

GMAO: Global Modeling and Assimilation Office, MERRA−2inst1_2d_int_Nx:2d, 1-Hourly, Instantaneous, Single-Level, Assimilation, Vertically Integrated Diagnostics V5.12.4. Greenbelt, MD, USA. Goddard Earth Sciences Data and Information Services Center (GES DISC), Accessed: 10-27-2016, https://doi.org/10.5067/G0U6NGQ3BLE0, 2015.

Heise, S., Dick, G., Gendt, G., Schmidt, T., and Wickert, J.: Integrated water vapor from IGS ground-based GPS observations: initial results from a global 5-min data set, Annales Geophysicae, 27, 2851–2859, https://doi.org/10.5194/angeo-27-2851-2009, 2009.

Hofmann-Wellenhof, B. and Moritz, H.: Physical geodesy, Springer Science & Business Media, 2006.

Ning, T., Elgered, G., Willén, U., and Johansson, J. M.: Evaluation of the atmospheric water vapor content in a regional climate model using ground-based GPS measurements, Journal of Geophysical Research: Atmospheres, 118, 329–339, https://doi.org/10.1029/2012jd018053, 2013.

Pavlis, N. K., Holmes, S. A., Kenyon, S. C., and Factor, J. K.: The development and evaluation of the Earth Gravitational Model 2008 (EGM2008), Journal of geophysical research: solid earth, 117, 2012.

Rienecker, M. M., Suarez, M. J., Gelaro, R., Todling, R., Bacmeister, J., Liu, E., Bosilovich, M. G., Schubert, S. D., Takacs, L., Kim, G.-K., and et al.: MERRA: NASA's Modern-Era Retrospective Analysis for Research and Applications, Journal of Climate, 24, 3624–3648, https://doi.org/10.1175/jcli-d-11-00015.1, 2011.

Teke, K., Nilsson, T., Böhm, J., Hobiger, T., Steigenberger, P., García-Espada, S., Haas, R., and Willis, P.: Troposphere delays from space geodetic techniques, water vapor radiometers, and numerical weather models over a series of continuous VLBI campaigns, Journal of Geodesy, 87, 981–1001, https://doi.org/10.1007/s00190-013-0662-z, 2013.

Tsidu, G. M., Blumenstock, T., and Hase, F.: Observations of precipitable water vapour over complex topography of Ethiopia from ground-based GPS, FTIR, radiosonde and ERA-Interim reanalysis, Atmospheric Measurement Techniques, 8, 3277–3295, https://doi.org/10.5194/amt-8-3277-2015, 2015.

van Dam, T., Altamimi, Z., Collilieux, X., and Ray, J.: Topographically induced height errors in predicted atmospheric loading effects, Journal of Geophysical Research, 115, https://doi.org/10.1029/2009jb006810, 2010.

Van Malderen, R., Brenot, H., Pottiaux, E., Beirle, S., Hermans, C., Mazière, M. D., Wagner, T., Backer, H. D., and Bruyninx, C.: A multi-site intercomparison of integrated water vapour observations for climate change analysis, Atmospheric Measurement Techniques, 7, 2487–2512, https://doi.org/10.5194/amt-7-2487-2014, 2014.

Wang, Y., Zhang, Y., Fu, Y., Li, R., and Yang, Y.: A climatological comparison of column-integrated water vapor for the third-generation reanalysis datasets, Science China Earth Sciences, 59, 296–306, https://doi.org/10.1007/s11430-015-5183-6, 2015.

Zhu, J.-H., S.-P. M. H. Z. L. Z. L. P.: Evaluation of reanalysis products with in situ GPS sounding observations in the Eastern Himalayas, Atmos. Oceanic Sci. Lett., 7, 17–22, https://doi.org/10.3878/j.issn.1674-2834.13.0050, 2014.

Table 1: Geopotential values at the selected GNSS stations. Values of z_{NWM} come from a bi-linear interpolation of the z^i_{NWM} around the GNSS site.

				Geopotential $[m^2s^{-2}]$		
	Station name	**Longitude** $[^\circ]$	**Latitude** $[^\circ]$	**GNSS**	**ERA-Interim**	**MERRA-2**
1	ACYA	-99.9030	16.8380	44.39	4173.38	1640.07
2	AREQ	-71.4928	-16.4655	24017.16	26377.14	37127.97
3	AUTF	-68.3036	-54.8395	575.91	2263.45	3335.30
4	AZUL	-59.8813	-36.7670	1385.73	1363.22	1348.82
5	BELE	-48.4626	-1.4088	336.47	172.74	127.65
6	BOAV	-60.7011	2.8452	831.69	1188.44	1130.29
7	BOGT	-74.0809	4.6401	25041.65	18524.49	19392.76
8	BRAZ	-47.8779	-15.9475	10969.77	9439.90	8995.93
9	BRFT	-38.4255	-3.8774	299.60	678.24	267.13
10	BRMU	-64.6963	32.3704	204.11	3.35	0.56
11	BYSP	-66.1612	18.4078	915.55	550.71	1651.25
12	CEFE	-40.3195	-20.3108	212.34	1760.98	2224.20
13	CHET	-88.2992	18.4953	96.56	360.99	184.30
14	CHPI	-44.9852	-22.6871	6087.93	8681.95	8612.77
15	CONZ	-73.0255	-36.8438	1571.61	1155.27	854.99
16	COPO	-70.3382	-27.3845	4392.35	12005.22	10847.58
17	CRO1	-64.5843	17.7569	114.90	-14.65	10.92
18	CUCU	-72.4879	7.8985	3049.05	11058.51	15115.12
19	CUIB	-56.0699	-15.5553	2306.02	2816.20	1992.91
20	EBYP	-55.8922	-27.3689	1261.19	1279.02	1482.36
21	FALK	-57.8741	-51.6937	379.44	71.21	142.72
22	GUAT	-90.5202	14.5904	14879.81	10900.60	13573.94
23	IGM1	-58.4393	-34.5722	340.41	179.50	188.85
24	ISPA	-109.3444	-27.1250	1140.45	12.21	14.73
25	LPAZ	-110.3194	24.1388	255.90	1022.71	941.86
26	LPGS	-57.9323	-34.9067	136.54	152.25	113.82
27	MABA	-49.1223	-5.3624	1012.82	1211.46	1384.44
28	MANA	-86.2490	12.1489	651.27	1754.72	2208.38
29	MAPA	-51.0973	0.0467	195.73	257.06	375.54

Table 1: Geopotential values at the selected GNSS stations. Values of z_{NWM} come from a bi-linear interpolation of the z^i_{NWM} around the GNSS site.

				Geopotential $[m^2s^{-2}]$		
	Station name	**Longitude** $[^\circ]$	**Latitude** $[^\circ]$	**GNSS**	**ERA-Interim**	**MERRA-2**
30	MARA	-71.6244	10.6740	419.77	713.91	432.58
31	MDO1	-104.0150	30.6805	19873.83	12481.26	12736.71
32	MERI	-89.6203	20.9800	209.13	137.52	263.13
33	MGBH	-43.9249	-19.9419	9618.59	8782.91	8625.43
34	MSCG	-54.5407	-20.4409	6615.27	4368.70	4816.39
35	MZAC	-68.8756	-32.8952	8208.77	15884.06	13487.88
36	NAUS	-60.0550	-3.0229	1036.87	462.89	314.52
37	OHI2	-57.9013	-63.3211	92.44	1206.90	1015.03
38	ONRJ	-43.2243	-22.8957	405.14	1879.10	3463.19
39	PALM	-64.0511	-64.7751	137.97	1968.40	1953.53
40	PARC	-70.8799	-53.1370	119.62	1391.48	1077.39
41	PBCG	-35.9071	-7.2137	5276.76	3525.56	3735.40
42	PEPE	-40.5061	-9.3844	3749.05	4542.51	4201.21
43	POAL	-51.1198	-30.0740	703.23	1251.90	272.29
44	POLI	-46.7303	-23.5556	7196.92	6505.10	4637.29
45	POVE	-63.8963	-8.7093	1055.27	954.44	960.02
46	PPTE	-51.4085	-22.1199	4276.27	3723.97	3862.36
47	RECF	-34.9515	-8.0510	252.14	936.50	419.74
48	RIO2	-67.7511	-53.7855	190.91	1005.86	465.51
49	RIOB	-67.8028	-9.9655	1448.38	1821.43	1706.42
50	RIOD	-43.3063	-22.8178	139.31	2320.91	2974.62
51	RNNA	-35.2077	-5.8361	498.84	512.19	355.41
52	SALU	-44.2125	-2.5935	433.87	120.98	279.50
53	SANT	-70.6686	-33.1503	6817.30	17025.96	11607.44
54	SAVO	-38.4323	-12.9392	855.49	412.21	821.07
55	SCUB	-75.7623	20.0121	436.41	1349.92	1839.31
56	SMAR	-53.7166	-29.7189	1015.39	1997.81	1877.46
57	SSA1	-38.5165	-12.9752	87.63	458.08	964.71
58	SSIA	-89.1166	13.6971	6131.25	4298.95	5206.12

Table 1: Geopotential values at the selected GNSS stations. Values of z_{NWM} come from a bi-linear interpolation of the z^i_{NWM} around the GNSS site.

				Geopotential [$m^2 s^{-2}$]		
	Station name	**Longitude** [°]	**Latitude** [°]	**GNSS**	**ERA-Interim**	**MERRA-2**
59	TOPL	-48.3307	-10.1711	2691.80	2752.17	3404.11
60	TUCU	-65.2304	-26.8433	4474.96	9038.43	11323.47
61	UBER	-48.3170	-18.8895	7867.99	7229.77	7267.98
62	UCOR	-64.1935	-31.4350	4289.42	6202.16	7133.34
63	UFPR	-49.2310	-25.4484	9040.97	6861.53	7676.59
64	UNRO	-60.6284	-32.9594	488.75	406.20	293.76
65	UNSA	-65.4076	-24.7275	12007.06	19659.75	19240.00
66	VESL	-2.8418	-71.6738	8362.05	5632.21	7588.75
67	VITH	-64.9692	18.3433	479.43	74.04	36.58

Table 2: Differences of the mean values of IWV ($\Delta\overline{IWV}$ in $[kg\,m^{-2}]$) between GNSS and the NWM for the period 2007-2013 at 67 stations located in South America and Central America. The mean value ($\overline{IWV}$) from GNSS at each site is also given and SD refers to the standard deviation. $\Delta z = z_{GNSS} - z_{NWM}$ refers to the difference in the geopotential $[m^2 s^{-2}]$ at each GNSS station.

	GNSS		**ERA-Interim**		**MERRA-2**	
Name	$\overline{IWV}$	SD	Δz	$\Delta\overline{IWV}$	Δz	$\Delta\overline{IWV}$
ACYA	41.70	11.72	-4128.99	4.88	-1595.68	0.92
AREQ	11.03	6.59	-2359.98	0.33	-13110.80	2.27
AUTF	10.48	3.71	-1687.54	0.52	-2759.39	0.80
AZUL	16.97	8.01	22.50	-1.10	36.91	-1.10
BELE	49.59	6.57	163.73	0.39	208.82	-1.54
BOAV	50.20	5.62	-356.75	1.50	-298.60	-1.45
BOGT	19.54	3.14	6517.15	-6.87	5648.89	-8.52
BRAZ	26.52	9.77	1529.88	-2.03	1973.84	-3.54
BRFT	42.26	8.05	-378.63	1.10	32.47	-0.49
BRMU	29.69	11.61	200.75	-0.30	203.55	-0.89
BYSP	39.10	8.74	364.83	-0.79	-735.70	0.41
CEFE	37.60	10.75	-1548.64	2.64	-2011.86	2.27
CHET	41.82	10.45	-264.43	0.69	-87.74	-0.93
CHPI	29.71	10.21	-2594.01	2.03	-2524.84	1.31
CONZ	14.16	5.32	416.34	0.09	716.62	-0.35
COPO	11.91	5.27	-7612.87	3.18	-6455.23	2.49
CRO1	38.53	8.76	129.56	-0.79	103.98	-0.98
CUCU	43.08	5.59	-8009.46	10.53	-12066.07	10.35
CUIB	40.98	11.98	-510.19	0.82	313.11	-0.25
EBYP	28.69	12.91	-17.83	-0.68	-221.17	-1.15
FALK	10.91	3.95	308.23	-0.41	236.72	-0.68
GUAT	22.88	7.29	3979.21	-6.75	1305.86	-5.86
IGM1	19.86	9.41	160.92	-0.93	151.56	-0.53
ISPA	26.26	7.40	1128.23	0.61	1125.72	0.16
LPAZ	25.53	15.27	-766.81	0.47	-685.96	0.02
LPGS	19.63	9.37	-15.71	-0.66	22.72	-0.91
MABA	46.95	7.92	-198.65	0.37	-371.62	-1.31
MANA	44.93	9.57	-1103.45	2.27	-1557.11	2.38

Table 2: Differences of the mean values of IWV ($\Delta\overline{IWV}$ in $[kg\,m^{-2}]$) between GNSS and the NWM for the period 2007-2013 at 67 stations located in South America and Central America. The mean value ($\overline{IWV}$) from GNSS at each site is also given and SD refers to the standard deviation. $\Delta z = z_{GNSS} - z_{NWM}$ refers to the difference in the geopotential $[m^2 s^{-2}]$ at each GNSS station.

	GNSS		**ERA-Interim**		**MERRA-2**	
Name	$\overline{IWV}$	SD	Δz	$\Delta\overline{IWV}$	Δz	$\Delta\overline{IWV}$
MAPA	49.92	6.67	-61.33	0.25	-179.81	-0.51
MARA	47.96	8.04	-294.13	1.43	-12.80	-0.74
MDO1	10.15	7.49	7392.57	-5.34	7137.12	-5.39
MERI	38.85	10.79	71.60	0.13	-54.00	-0.58
MGBH	26.75	9.88	835.68	-1.00	993.17	-2.63
MSCG	31.75	10.81	2246.58	-2.74	1798.88	-3.37
MZAC	15.25	7.33	-7675.29	1.21	-5279.11	2.41
NAUS	47.44	5.97	573.97	-3.79	722.35	-5.89
OHI2	5.89	2.83	-1114.46	-0.53	-922.59	-1.03
ONRJ	36.33	11.44	-1473.97	2.01	-3058.05	3.12
PALM	6.78	3.03	-1830.43	0.54	-1815.56	0.21
PARC	10.24	4.04	-1271.86	-0.82	-957.77	-1.23
PBCG	33.55	7.50	1751.20	0.23	1541.36	-0.20
PEPE	33.48	8.15	-793.46	1.42	-452.16	-0.49
POAL	26.68	11.03	-548.67	0.95	430.94	0.19
POLI	27.42	10.39	691.82	-1.11	2559.63	-4.53
POVE	50.42	8.68	100.82	0.76	95.25	-0.80
PPTE	30.92	11.81	552.29	-1.33	413.91	-2.08
RECF	38.96	7.87	-684.35	2.20	-167.60	2.15
RIO2	9.80	3.88	-814.94	-0.87	-274.59	-1.52
RIOB	46.91	8.37	-373.0	-0.82	-258.04	-2.86
RIOD	37.82	11.60	-2181.60	3.50	-2835.31	3.67
RNNA	40.09	8.38	-13.35	1.10	143.43	0.31
SALU	47.88	6.89	312.88	0.53	154.37	-1.02
SANT	12.51	4.91	-10208.66	5.53	-4790.14	4.07
SAVO	35.72	8.15	443.27	-0.42	34.92	0.10
SCUB	37.84	9.85	-913.51	0.00	-1402.90	0.96
SMAR	25.92	11.46	-982.43	0.46	-862.07	0.11

Table 2: Differences of the mean values of IWV ($\Delta\overline{IWV}$ in $[kg\,m^{-2}]$) between GNSS and the NWM for the period 2007-2013 at 67 stations located in South America and Central America. The mean value ($\overline{IWV}$) from GNSS at each site is also given and SD refers to the standard deviation. $\Delta z = z_{GNSS} - z_{NWM}$ refers to the difference in the geopotential $[m^2 s^{-2}]$ at each GNSS station.

	GNSS		**ERA-Interim**		**MERRA-2**	
Name	$\overline{IWV}$	SD	Δz	$\Delta\overline{IWV}$	Δz	$\Delta\overline{IWV}$
SSA1	36.80	8.36	-370.45	0.72	-877.07	1.30
SSIA	36.46	8.42	1832.30	-3.34	925.13	-3.92
TOPL	40.69	11.33	-61.08	-0.05	-712.31	-0.22
TUCU	25.36	12.17	-4563.47	0.51	-6848.51	4.31
UBER	28.03	10.83	638.22	-2.24	600.02	-3.36
UCOR	18.77	9.78	-1912.73	-0.93	-2843.92	0.32
UFPR	23.77	9.64	2179.43	-2.78	1364.38	-3.91
UNRO	21.74	10.52	82.54	-0.64	194.99	-0.51
UNSA	19.71	10.01	-7652.70	2.50	-7232.94	3.68
VESL	3.17	1.29	2729.84	1.03	773.30	1.07
VITH	39.08	8.75	405.39	-0.72	442.85	-0.74

Table 3: Mean values of the difference between $IWV_{ERAInterim}$ data and IWV computed from the numerical integral of the equation 7 at each grid point surrounding the GNSS site. The integration limits range from 1 hPa to the static geopotential value assigned by ERA Interim to the point ($z^i_{ERAInterim}$).

Station name	**NorthWest**		**NorthEast**		**SouthWest**		**SouthEast**	
	mean	**sd**	**mean**	**sd**	**mean**	**sd**	**mean**	**sd**
ACYA	-0.37	0.39	-0.19	0.34	-0.49	0.36	-0.39	0.36
AREQ	0.13	0.74	0.15	0.53	-0.12	0.32	0.00	0.33
AUTF	0.04	0.03	0.05	0.07	0.04	0.04	0.04	0.04
AZUL	0.06	0.06	0.06	0.07	0.06	0.06	0.06	0.09
BELE	0.15	0.08	0.17	0.1	0.15	0.09	0.19	0.18
BOAV	0.15	0.12	0.15	0.08	0.15	0.14	0.14	0.08
BOGT	-0.21	0.26	-0.05	0.12	0.14	0.11	0.08	0.11
BRAZ	0.14	0.09	0.14	0.09	0.15	0.11	0.14	0.09
BRFT	0.14	0.09	0.14	0.14	0.14	0.10	0.12	0.16
BRMU	0.11	0.09	0.12	0.08	0.09	0.09	0.11	0.08
BYSP	0.14	0.08	0.15	0.08	0.13	0.08	0.13	0.09
CEFE	0.08	0.13	0.12	0.08	0.09	0.22	0.14	0.11
CHET	0.14	0.11	0.15	0.12	0.14	0.09	0.16	0.24
CHPI	0.00	0.23	0.03	0.12	0.05	0.09	0.08	0.08
CONZ	0.05	0.05	0.02	0.07	0.03	0.05	0.00	0.10
COPO	-0.02	0.07	-0.92	0.53	-0.03	0.07	-0.55	0.52
CRO1	0.16	0.08	0.17	0.11	0.15	0.09	0.16	0.09
CUCU	0.21	0.20	0.55	0.22	0.01	0.29	0.56	0.40
CUIB	0.17	0.09	0.12	0.14	0.15	0.09	0.15	0.08
EBYP	0.11	0.22	0.11	0.13	0.11	0.13	0.11	0.21
FALK	0.04	0.03	0.04	0.05	0.04	0.03	0.04	0.08
GUAT	0.04	0.24	-0.17	0.24	0.06	0.14	0.00	0.11
IGM1	0.07	0.08	0.07	0.11	0.09	0.08	0.08	0.07
ISPA	0.09	0.08	0.09	0.09	0.10	0.08	0.09	0.12
LPAZ	0.05	0.07	0.03	0.08	0.05	0.09	0.03	0.10
LPGS	0.08	0.08	0.04	0.10	0.13	0.23	0.09	0.16
MABA	0.18	0.10	0.17	0.09	0.16	0.09	0.17	0.21
MANA	0.16	0.07	0.17	0.07	0.15	0.23	0.13	0.16
MAPA	0.14	0.07	0.14	0.09	0.15	0.09	0.14	0.19

Table 3: Mean values of the difference between $IWV_{ERAInterim}$ data and IWV computed from the numerical integral of the equation 7 at each grid point surrounding the GNSS site. The integration limits range from 1 hPa to the static geopotential value assigned by ERA Interim to the point ($z^i_{ERAInterim}$).

Station name	**NorthWest**		**NorthEast**		**SouthWest**		**SouthEast**	
	mean	**sd**	**mean**	**sd**	**mean**	**sd**	**mean**	**sd**
MARA	0.16	0.06	0.16	0.13	0.12	0.07	0.21	0.34
MDO1	0.06	0.06	0.11	0.22	0.05	0.06	0.04	0.07
MERI	0.17	0.24	0.11	0.18	0.19	0.11	0.14	0.09
MGBH	0.13	0.11	0.10	0.15	0.12	0.11	0.12	0.09
MSCG	0.12	0.09	0.12	0.12	0.12	0.09	0.10	0.18
MZAC	-0.53	0.63	0.05	0.16	-0.19	0.53	0.04	0.16
NAUS	0.17	0.09	0.19	0.13	0.15	0.08	0.15	0.09
OHI2	0.00	0.04	0.01	0.02	0.02	0.01	0.02	0.01
ONRJ	0.10	0.08	0.09	0.08	0.11	0.11	0.08	0.09
PALM	0.01	0.05	0.00	0.07	-0.01	0.04	-0.02	0.04
PARC	0.04	0.02	0.04	0.02	0.04	0.02	0.04	0.07
PBCG	0.15	0.12	0.13	0.11	0.16	0.14	0.13	0.14
PEPE	0.16	0.10	0.19	0.18	0.17	0.11	0.16	0.10
POAL	0.12	0.13	0.08	0.07	0.17	0.27	0.07	0.08
POLI	0.12	0.08	0.11	0.08	0.08	0.16	0.00	0.18
POVE	0.17	0.14	0.19	0.20	0.17	0.14	0.17	0.13
PPTE	0.12	0.10	0.12	0.08	0.11	0.12	0.11	0.08
RECF	0.09	0.11	0.09	0.11	0.12	0.17	0.12	0.13
RIO2	0.03	0.03	0.04	0.02	0.02	0.06	0.02	0.02
RIOB	0.14	0.11	0.14	0.18	0.15	0.15	0.13	0.09
RIOD	0.10	0.08	0.10	0.08	0.12	0.13	0.11	0.10
RNNA	0.09	0.10	0.10	0.12	0.13	0.09	0.13	0.09
SALU	0.16	0.09	0.15	0.10	0.17	0.10	0.14	0.17
SANT	-0.30	0.48	-0.03	0.23	-0.42	0.45	0.00	0.23
SAVO	0.13	0.19	0.16	0.17	0.13	0.10	0.15	0.09
SCUB	0.12	0.23	0.13	0.11	0.14	0.07	0.14	0.07
SMAR	0.12	0.16	0.12	0.18	0.10	0.08	0.10	0.09
SSA1	0.16	0.12	0.14	0.19	0.12	0.10	0.15	0.09
SSIA	0.06	0.12	0.08	0.11	-0.01	0.15	0.00	0.25

Table 3: Mean values of the difference between $IWV_{ERAInterim}$ data and IWV computed from the numerical integral of the equation 7 at each grid point surrounding the GNSS site. The integration limits range from 1 hPa to the static geopotential value assigned by ERA Interim to the point ($z^i_{ERAInterim}$).

Station name	**NorthWest**		**NorthEast**		**SouthWest**		**SouthEast**	
	mean	**sd**	**mean**	**sd**	**mean**	**sd**	**mean**	**sd**
TOPL	0.18	0.09	0.19	0.16	0.18	0.10	0.17	0.12
TUCU	0.11	0.11	0.14	0.43	0.12	0.09	0.19	0.21
UBER	0.15	0.14	0.15	0.08	0.16	0.15	0.15	0.08
UCOR	0.09	0.10	0.07	0.09	0.07	0.16	0.04	0.22
UFPR	0.02	0.17	0.04	0.10	0.03	0.11	0.03	0.09
UNRO	0.08	0.08	0.06	0.08	0.08	0.08	0.05	0.07
UNSA	-0.27	0.25	-0.63	0.43	-0.55	0.32	-0.59	0.52
VESL	-0.03	0.05	-0.03	0.05	-0.02	0.04	-0.02	0.05
VITH	0.15	0.10	0.17	0.09	0.13	0.15	0.15	0.09

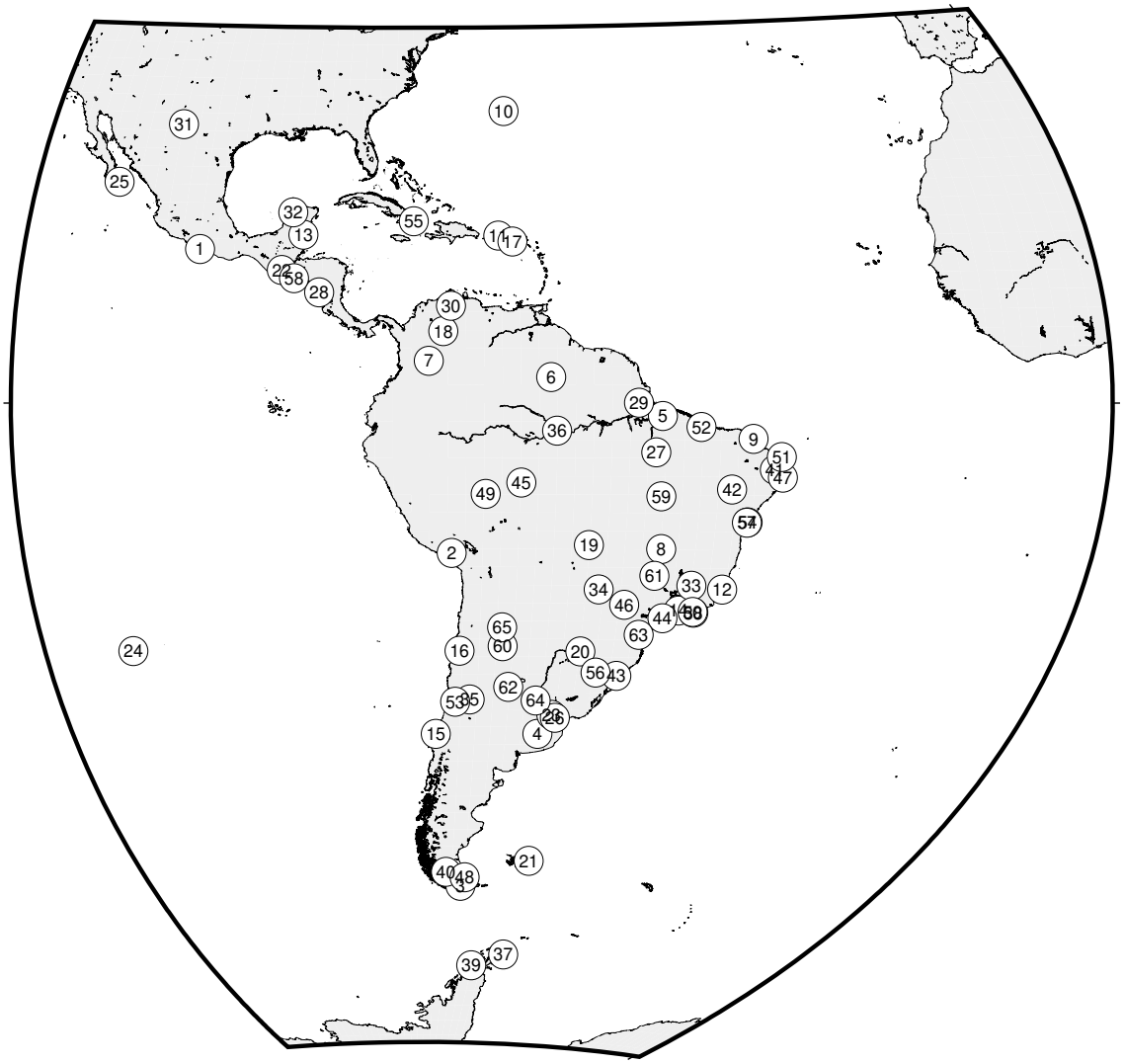

Figure 1. Location of the GNSS stations (see Table 1).

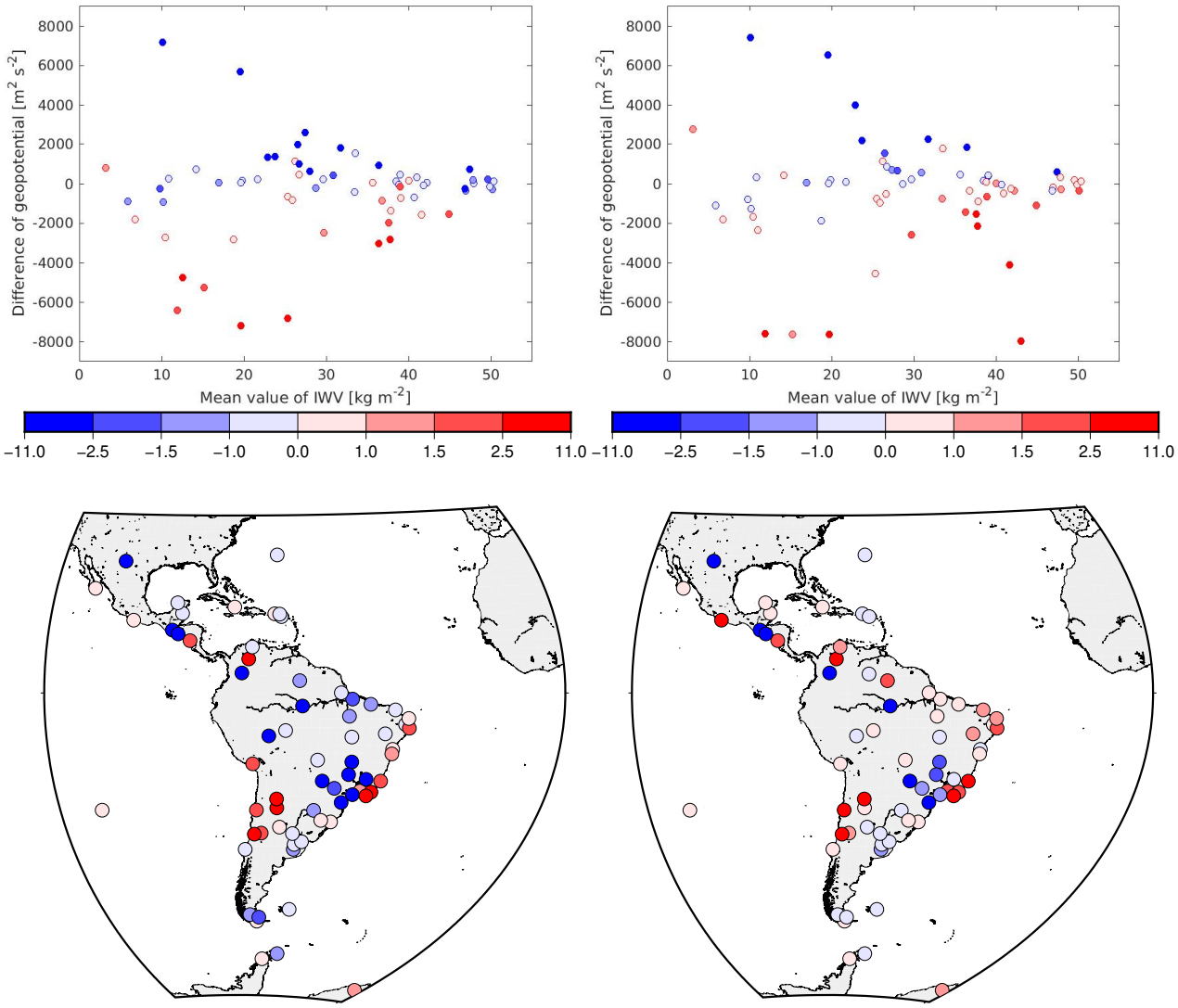

Figure 2. (up) Geopotential differences Δz as a function of the mean values of IWV from GNSS ($\overline{IWV}_{GNSS}$). Results for MERRA-2 are on the left and the same for ERA Interim on the right. Different color dots indicate values of $\Delta\overline{IWV} = \overline{IWV}_{GNSS} - \overline{IWV}_{ERA\,Interim}$. (down) Geographical distribution of $\Delta\overline{IWV}$ for MERRA-2 (left) and ERA Interim (right).

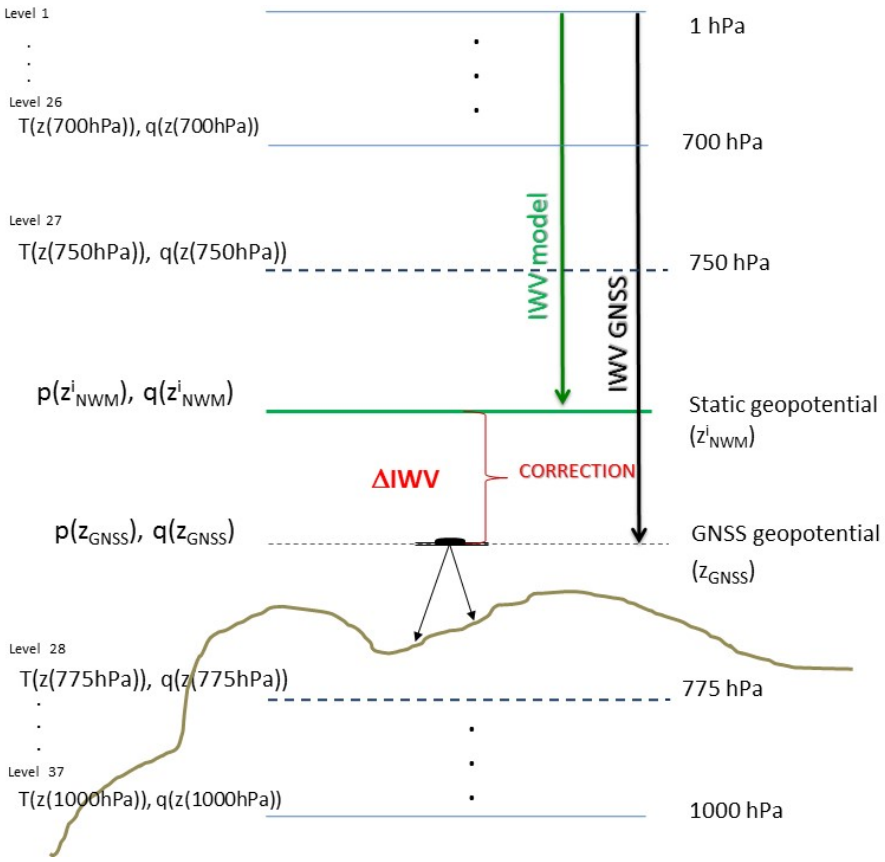

Figure 3. Scheme of the applied correction to the IWV from ERA-Interim reanalysis. Both unknowns (z_{GNSS}, dark blue dashed line and z^i_{NWM}, thick green line) are located between the pressure levels 27 (750 hPa) and 28 (775 hPa) indicated with thick dashed lines. Atmospheric pressure (p), temperature (T) and specific humidity (q) are known in the 37 levels from 1 hPa till 1000 hPa.

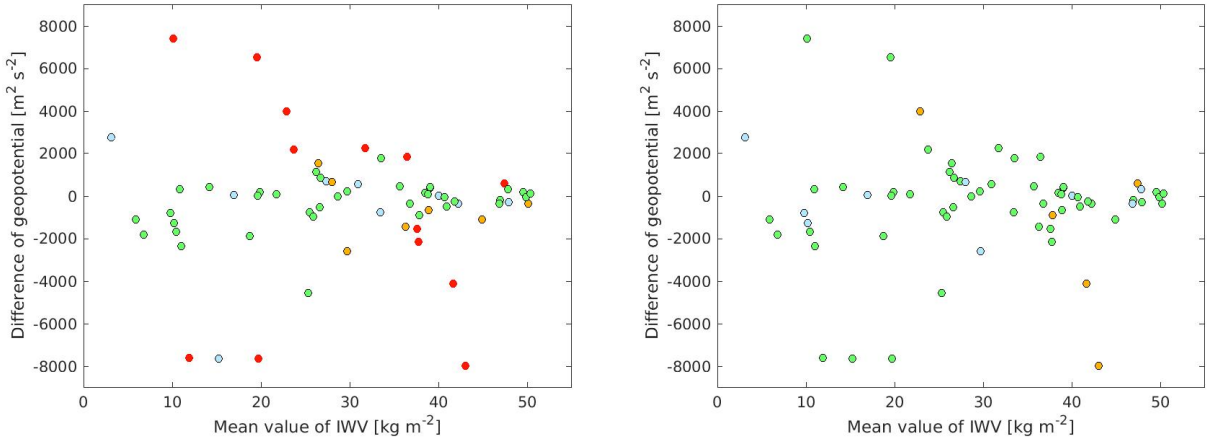

Figure 4. Δz as function of $\overline{IWV}_{GNSS}$. The different color dots indicate the value of the differences between averages of GNSS and ERA Interim ($\left|\Delta\overline{IWV}\right| = \left|\overline{IWV}_{GNSS} - \overline{IWV}_{ERAInterim}\right|$) : green for $\left|\Delta\overline{IWV}\right| \leq 1\ kg\ m^{-2}$, light blue for $1\ kg\ m^{-2} \leq \left|\Delta\overline{IWV}\right| \leq 1.5\ kg\ m^{-2}$, orange for $1.5\ kg\ m^{-2} < \left|\Delta\overline{IWV}\right| \leq 2.5\ kgm^{-2}$ and red for $\left|\Delta\overline{IWV}\right| \geq 2.5\ kg\ m^{-2}$. Results before applying the integral correction are shown on the left and after the correction on the right.

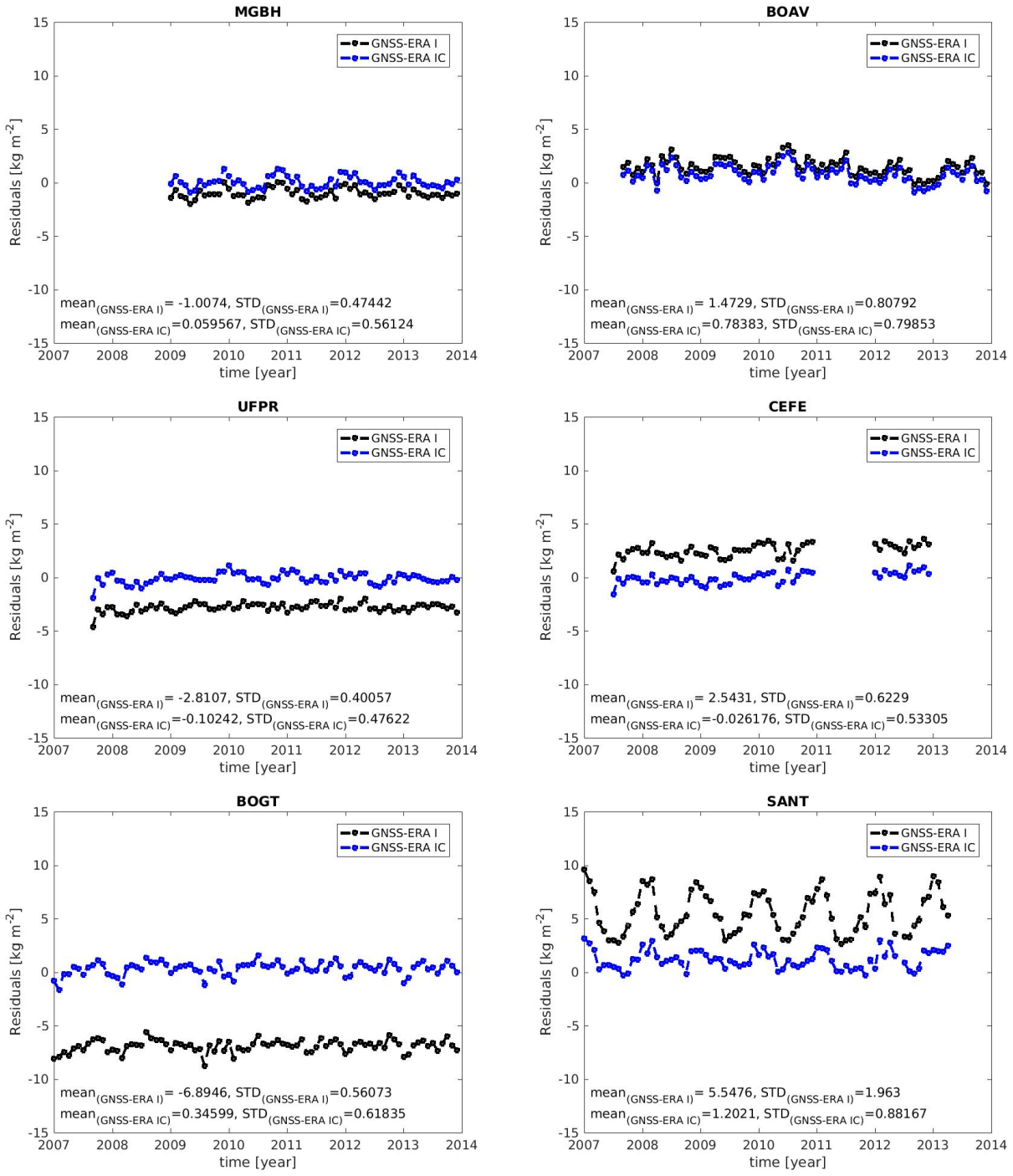

Figure 5. Residuals of the difference $(IWV_{GNSS} - IWV_{ERAInterim})$ (GNSS - ERA I, black line) along with residuals of the difference $[IWV_{GNSS} - (IWV_{ERAInterim} + correction)]$ (GNSS - ERA IC, blue line). Left column shows stations with positive Δz, it means that GNSS station is higher to the location assigned by ERA-Interim, and the opposite is at the right column. Mean values of the residuals along with the standard deviations are also provided. The sites are shown according to Δz decreasing from top to bottom at each column.

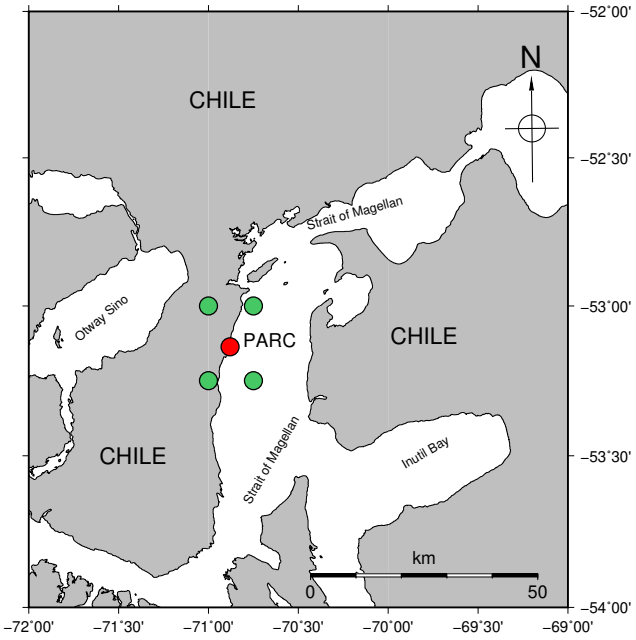

Figure 6. Location of GNSS station PARC along with the 4 grid points around the station. The grid points correspond to ERA-Interim.